AIAA JOURNAL
Vol. 34, No. 3, March 1996

Spectral Solution of the Viscous Blunt-Body Problem 2: Multidomain Approximation

David A. Kopriva*
Florida State University, Tallahassee, Florida 32306

We present steady solutions of high-speed viscous flows over blunt bodies using a multidomain Chebyshev spectral collocation method. The region within the shock layer is divided into subdomains so that internal layers can be well resolved. In the interiors of the subdomains, the solution is approximated by Chebyshev collocation. At interfaces between subdomains, the advective terms are upwinded and the viscous terms are treated by a penalty method. The method is applied to five flows in the Mach number range 5–25 and Reynolds number range from 2×10^3 to 83×10^4, based on nose radius. Results are compared with experimental data and to a finite difference solution.

Introduction

SPECTRAL methods, characterized by high-order orthogonal polynomial approximations, are now applied to a wide variety of fluid dynamics problems.[1] For smooth enough solutions they give exponential order convergence. The spectral approximation of advective terms generates low dissipation errors, which is important in viscous flow calculations. Compared with finite difference methods, fewer grid points are needed by spectral methods to obtain highly accurate solutions.[2]

On the negative side, the use of global polynomial approximations makes it difficult to solve problems with multiple length scales. These scales might be associated with the size of an aerodynamic body, the distance between shock waves, the size of entropy and vorticity layers, and the size of viscous boundary layers. A standard spectral collocation method would require a complex mapping and a large number of grid points to solve such problems. Refinement of the grid to resolve local features would have to be handled by the mappings. The resulting problem would be numerically very stiff. Very small time steps and large numbers of iterations would be required to converge to steady state.

To ameliorate the difficulties of standard spectral methods, multidomain spectral methods have been developed to solve incompressible viscous (see Ref. 1 for a discussion) and, now, compressible[3–7] flows. Multidomain methods still give the exponential error convergence characteristic of the spectral methods but also allow for local refinement of the grid.

In this paper, we apply to the solution of the steady blunt-body problem a new multidomain Chebyshev collocation method developed for the solution of the compressible Navier–Stokes equations.[8] At a subdomain interface, the advective terms in the equations are treated by an upwind characteristic correction procedure developed for the inviscid Euler gasdynamics equations.[3] The viscous terms are approximated by a weighted average of the terms on either side plus a penalty term proportional to the jump in the viscous fluxes. The result is a method with communication limited to the passing of boundary data only.

The method is applied to five examples. The first four examples are of sphere, cylinder, and blunt cone geometries at Mach numbers 5.73 and 10.6. For these solutions, the surface pressure or the heat transfer are compared with experiments. The final problem is the solution of a Mach 25 flow over a hyperbolic cone. This problem was solved earlier by a single-domain spectral method.[9] The results are compared with a finite difference thin-layer Navier–Stokes calculation and to the single-domain solution.

Received Oct. 31, 1994; revision received April 27, 1995; accepted for publication May 6, 1995.

*Associate Professor, Department of Mathematics, and Supercomputer Computations Research Institute. Senior Member AIAA.

Blunt-Body Problem

In this paper we solve for viscous supersonic flow about a blunt nose cone at zero angle of attack.[9] Spectral approximations of this problem using single domains have been performed by Kopriva[9] and Wang et al.[10] Because of the symmetry along the centerline of the body, we need to solve only the upper half of the full flow problem. For high Mach and Reynolds numbers, the bow shock can be viewed as a discontinuity.[7] By fitting the shock as a boundary to the flow, then, we consider the solution only in the shock layer.

We approximate the compressible Navier–Stokes equations in the nonconservative form as written in Ref. 9. The pressure, density, and temperature, denoted here as p, ρ, and T, are scaled to the freestream values p_∞, ρ_∞, and T_∞. The velocities u and v are scaled to $\sqrt{(T_\infty)}$. The temperature is computed by the perfect gas equation of state. The experiments with which we compare had postshock temperatures of about 2000°R, well below the dissociation temperature of air. Thus, the ideal gas law should be acceptable, even though the Mach numbers are high. As before, we compute the viscosity coefficient by the Sutherland law.

Multidomain Spectral Method

The multidomain method that we use was presented in Ref. 8. In this paper, the geometry is allowed to change with time (because of the moving shock), and axisymmetric geometry is considered. The moving grid requires the interface conditions to change at each time step. The domain is decomposed for the blunt-body problem as described by Kopriva[4,5] for the inviscid case. All lengths are scaled to the nose radius.

On each subdomain, the Navier–Stokes equations can be rewritten as

$$\begin{aligned} \rho_\tau + A_\rho &= 0 \\ u_\tau + A_u &= V_u \\ v_\tau + A_v &= V_v \\ p_\tau + A_p &= V_p \end{aligned} \tag{1}$$

where A represents an advective term and V represents a viscous term.[8]

To approximate the equations, we place a grid of points

$$\left(X_i^k, Y_j^k\right) = \left\{\frac{1}{2}\left[1 - \cos\left(\frac{i\pi}{N^k}\right)\right], \frac{1}{2}\left[1 - \cos\left(\frac{j\pi}{M^k}\right)\right]\right\} \qquad \begin{aligned} i &= 0, 1, 2, \ldots, N^k \\ j &= 0, 1, 2, \ldots, M^k \end{aligned} \tag{2}$$

on each subdomain and assign gridpoint values of the solution

unknowns, e.g., $p^k_{i,j}$ etc. Derivatives of a solution variable, $q(= u, v,$ or $p)$, are then approximated from the grid point values $q_{i,j}$ by

$$\begin{aligned}\left(q^k_X\right)_{i,j} &\approx \sum_{l=0}^{N^k} \mathrm{d}^{(X)}_{i,l} q^k_{l,j} \\ \left(q^k_Y\right)_{i,j} &\approx \sum_{l=0}^{M^k} \mathrm{d}^{(Y)}_{j,l} q^k_{i,l}\end{aligned} \tag{3}$$

where $\mathrm{d}_{i,j}$ is the Chebyshev derivative matrix (Ref. 1, p. 69). We use matrix multiplication rather than fast Fourier transforms (FFTs) to compute the derivative approximation, and the total number of points is kept less than the break-even number of points where the FFTs become faster.[1]

The derivative approximations (3) are substituted into Eqs. (1) to give a system of ordinary differential equations, which we denote by

$$\frac{\partial \rho^k_{i,j}}{\partial t} = -(A_\rho)^k_{i,j} \tag{4a}$$

and for $q =$ each of p, u, or v,

$$\frac{\mathrm{d}q^k_{i,j}}{\mathrm{d}t} = -(A_q)^k_{i,j} + (V_q)^k_{i,j} \tag{4b}$$

These equations are integrated in time with a second-order Runge–Kutta rule.

At interfaces between the subdomains, conditions are applied to allow waves to propagate through them, while weakly enforcing continuity of the viscous flux. To describe the interface method,[8] we consider two subdomains as shown in Fig. 1, one on the left (L) and the other on the right (R) of the interface.

Since we replace the spatial derivatives in Eq. (1) by their discrete Chebyshev approximations, two equations are generated for each interface point. One uses derivatives computed from the left, and the other uses derivatives computed from the right. For the density, the equation is purely advective, and we write

$$\begin{aligned}\frac{\partial \rho^L_{N^L,j}}{\partial t} &= -(A_\rho)^L_{N^L,j} \\ \frac{\partial \rho^R_{0,j}}{\partial t} &= -(A_\rho)^R_{0,j}\end{aligned} \tag{5a}$$

For $q =$ each of p, u, and v, the equations on either side of the interface are written so that the viscosity is approximated by a weighted average of the viscous terms computed on either side of the interface. The continuity required of the viscous flux is enforced weakly by a penalty proportional to the jump in the flux:

$$\begin{aligned}\frac{\mathrm{d}q^L_{N^L,j}}{\mathrm{d}t} &= -(A_q)^L_{N^L,j} + \alpha_j (V_q)^L_{N^L,j} + \beta_j (V_q)^R_{0,j} \\ &\quad + \delta_j \left(\tilde{F}^R_{q_{0,j}} - \tilde{F}^L_{q_{N^L,j}}\right) \\ \frac{\mathrm{d}q^R_{0,j}}{\mathrm{d}t} &= -(A_q)^R_{0,j} + \alpha_j (V_q)^L_{N^L,j} + \beta_j (V_q)^R_{0,j} \\ &\quad + \delta_j \left(\tilde{F}^R_{q_{0,j}} - \tilde{F}^L_{q_{N^L,j}}\right)\end{aligned} \tag{5b}$$

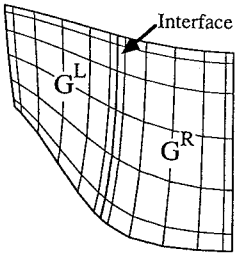

Fig. 1 Diagram of a two-subdomain decomposition.

where $\tilde{F}$ is the contravariant viscous flux. The weights α, β, and δ depend on the relative sizes of the subdomains and on the numbers of points in the subdomains:

$$\begin{aligned}\alpha_j &= \frac{J^L_{N^L,j} w^L_{N^L}}{J^L_{N^L,j} w^L_{N^L} + J^R_{0,j} w^R_0} \\ \beta_j &= \frac{J^R_{0,j} w^R_0}{J^L_{N^L,j} w^L_{N^L} + J^R_{0,j} w^R_0} \\ \delta_j &= \frac{1}{J^L_{N^L,j} w^L_{N^L} + J^R_{0,j} w^R_0}\end{aligned} \tag{6}$$

The quantities

$$w^R_0 = \frac{1}{2[(N^R)^2 - 1]}, \qquad w^L_{N^L} = \frac{1}{2[(N^L)^2 - 1]}$$

are the Clenshaw–Curtis quadrature weights defined on the interval $[0, 1]$. To update the solutions, Eqs. (5) are integrated with a second-order Runge–Kutta rule.

An approximation similar to Eq. (5) can be written for corner points found at the intersection of four subdomains.[8] At such points, the weighted average is taken over the four values of the diffusion terms, and penalties are applied for the jumps in the diffusive fluxes across each face.

The results of the integration in time are preliminary values of the solutions $\tilde{\rho}$, $\tilde{p}$, $\tilde{u}$, and $\tilde{v}$ on either side of the interface. The preliminary values have used one-sided, but not upwind, approximations for the advective terms at the interface points. Thus, these solutions must be corrected to account for wave propagation across the interface. From $\tilde{u}$ and $\tilde{v}$, preliminary values of the normal and tangential velocities $\tilde{w}_1$ and $\tilde{w}_2$ are formed. The preliminary values are then corrected to have the proper advective domain of dependence in the manner described in Ref. 3. For instance, if the flow is subsonic, and from left to right across the interface, the choice of four bicharacteristics of the hyperbolic portion of the equations leads to the corrected interface values

$$\begin{aligned}p^L_{N^L,j} = p^R_{0,j} &= \tfrac{1}{2}\left(\tilde{p}^L_{N^L,j} + \tilde{p}^R_{0,j}\right) + \rho^n a^n \left[(\tilde{w}_1)^L_{N^L,j} - (\tilde{w}_1)^R_{0,j}\right] \\ (w_1)^L_{N^L,j} = (w_1)^R_{0,j} &= \tfrac{1}{2}\left[(\tilde{w}_1)^L_{N^L,j} + (\tilde{w}_1)^R_{0,j}\right] \\ &\quad + \frac{1}{\rho^n a^n}\left(\tilde{p}^L_{N^L,j} - \tilde{p}^R_{0,j}\right) \\ (w_2)^L_{N^L,j} &= (w_2)^R_{0,j} = (w_2)^L_{N^L,j} \\ \rho^L_{N^L,j} = \rho^R_{0,j} &= \tilde{\rho}^L_{N^L,j} + \frac{1}{(a^n)^2}\left(p^L_{N^L,j} - \tilde{p}^L_{N^L,j}\right)\end{aligned} \tag{7}$$

The superscript n refers to the linearization to the previous time level. The velocities u and v can then be computed from the corrected normal and tangential velocities w_1 and w_2.

The boundary conditions and their approximations are described in detail in Ref. 9. We will only review the basic ideas here. To compute the wall pressure, we use a compatibility equation that relates the pressure and the normal velocity along the inviscid characteristic direction. Thus, the pressure is required to satisfy a combination of both the energy and momentum equations at the body surface. If the surface is adiabatic, this equation uses the normal temperature gradient set equal to zero when the second derivative is computed. The density is computed from the pressure and the temperature either from the equation of state, for an isothermal surface, or, for an adiabatic surface, by a spectral extrapolation that enforces the zero normal temperature gradient.

The shock boundary is treated as a discontinuity by shock fitting since at high Mach and Reynolds numbers the shock can be considered a sharp discontinuity.[11] The shock-fitting procedure is described in detail in Ref. 4 for the inviscid case. The sharp shock assumption implies that the viscous terms are negligible near the shock, so we ignore them in the calculation of the downstream pressure.

At the outflow boundary, we impose the viscous conditions by setting the normal viscous fluxes to be zero when the second derivatives

are computed. Since the streamwise flux is small in high-Reynolds-number flow, this has little effect on the solution. In the subsonic portion of the boundary layer, we also specify the pressure to be a fixed value and typically use the inviscid pressure. That pressure can be obtained from a Newtonian flow assumption, which is reasonably accurate for hypersonic flows. It can also be obtained from the solution of the inviscid equations, which we use to start the viscous computation.

Unlike the solutions presented in Ref. 10, no artificial viscosity or spectral filtering are used with this approximation. Filtering of the solution either directly or by the addition of artificial viscous terms is undesirable for three reasons. First, the overall accuracy of the approximation is decreased, since the number of accurate frequencies is reduced. Second, high-frequency information is altered. Finally, artificial viscous effects can be introduced in the solution. In the absence of shocks or other discontinuities in the computed region, which we avoid here by shock fitting, the need for explicit filtering of smooth solutions often indicates the use of poor boundary procedures that introduce high-frequency errors into the solution. These errors destroy both the solution accuracy and, in steady-state problems, the convergence rate.

Solutions

Five problems are solved using the method just described. A summary of the flow parameters is shown below in Table 1. The subscript w represents a wall value. The problems include both two-dimensional and axisymmetric flows at a range of Reynolds, Re, and Mach, M, numbers. The solutions for problems I–IV are compared with experimental data. The last problem compares the computed results with a finite difference solution.[12]

Case I

The first problem that we solve is the $M = 10.6$ flow over a sphere at Reynolds number 8.3×10^4 based on nose radius, using a grid with eight subdomains. Figure 2 shows the computed contours of the pressure, Mach number, and temperature along with the grid used. The narrow strip of subdomains along the surface of the sphere

Table 1 Parameters for the flow test cases

Case	Geometry	M_∞	Re	T_∞,° R	T_w/T_∞	Purpose
I	Sphere	10.6	8.33×10^4	85.21	Adiab.	Compute C_p
II	Cylinder	5.73	2.050×10^3	71.37	71.37	Heat transfer
III	15-deg sphere/cone	10.6	8.33×10^4	85.21	Adiab.	C_p
IV	15-deg sphere/cone	10.6	1.65×10^5	85.21	6.22	Heat transfer
V	5-deg hyperboloid	25	1.3034×10^4	486	25	Compare with thin-layer solution

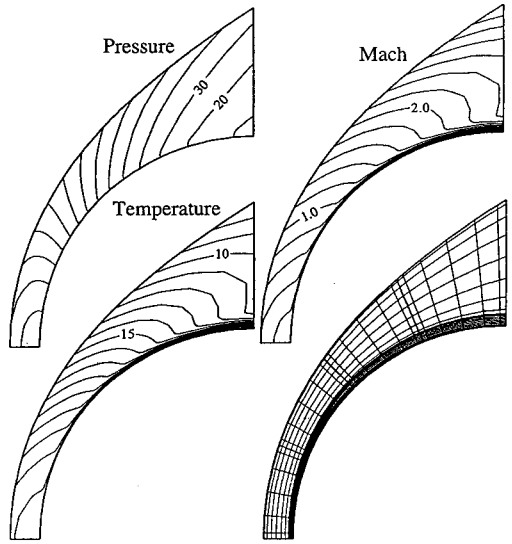

Fig. 2 Solution contours and grid for case I.

Table 2 Convergence of the stagnation pressure

N	Rel. error
4	2.6×10^{-2}
6	2.9×10^{-3}
8	7.6×10^{-5}

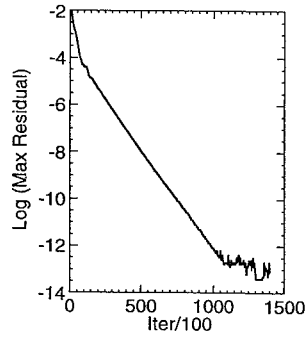

Fig. 3 Convergence of the residual for case I.

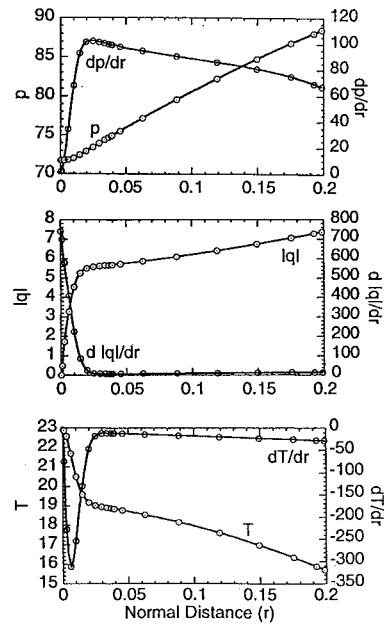

Fig. 4 Solution and derivative profiles at $s = 0.78$ for case I.

was chosen to better resolve the boundary layer. A coarse grid is all that is needed to resolve the essentially inviscid flow outside of the boundary layer. Convergence behavior of the maximum residual over all flow variables, plotted in Fig. 3, shows that steady state is obtained in double precision (64-bit) arithmetic.

One known quantity in the solution of this flow is the stagnation pressure. In Table 2, we show the convergence of the relative error in the stagnation pressure as the number of grid points per subdomain is increased. For this test, we used the same number of grid points N in each coordinate direction and in each subdomain. The convergence is spectral, and doubling the number of points from four to eight decreases the error by two and one-half orders of magnitude.

The solution contours are smooth and pass continuously through the interfaces. Normal direction profiles for the pressure, velocity and temperature and their derivatives are shown in Fig. 4, at a point approximately halfway along the surface of the sphere.

Finally, Fig. 5 plots the pressure coefficient

$$C_p = \frac{p_{\text{body}} - p_\infty}{(\gamma/2) p_\infty M_\infty^2}$$

along the surface of the sphere measured as horizontal distance from the leading edge. The result is compared with the inviscid solution computed in Ref. 5 and to the experimental data of Cleary.[13] The viscous computation clearly approximates the data better than the inviscid computation.

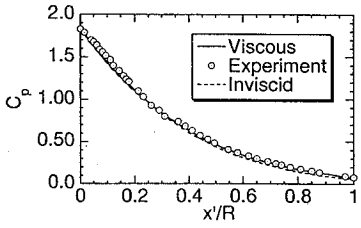

Fig. 5 Pressure coefficient for case I as a function of horizontal distance from the leading edge.

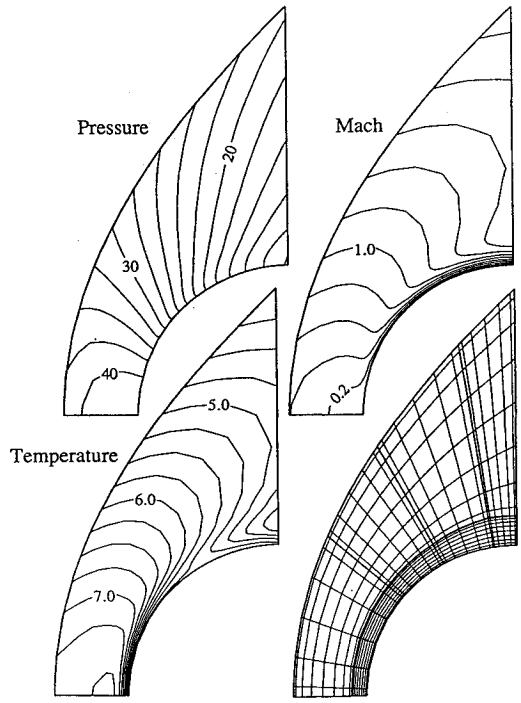

Fig. 6 Solution contours and grid for case II.

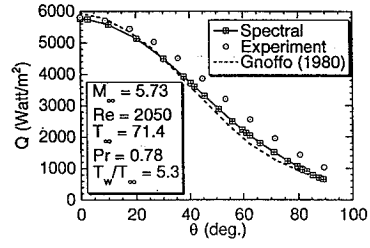

Fig. 7 Heat transfer along the cylinder surface for case II.

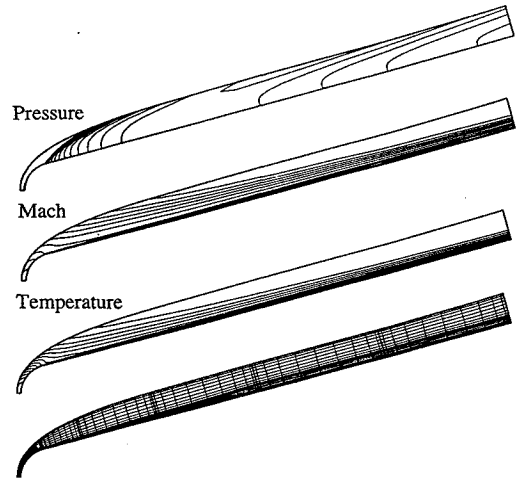

Fig. 8 Solution contours and grid for case III.

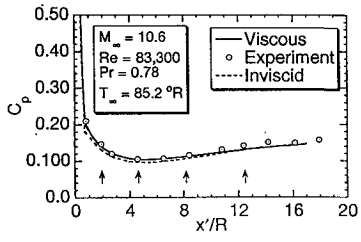

Fig. 9 Pressure coefficient along body surface for case III.

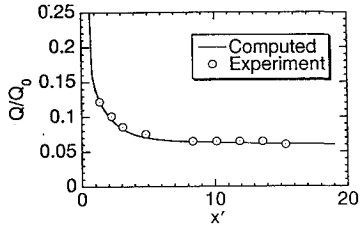

Fig. 10 Heat flux for case IV.

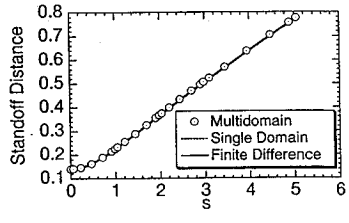

Fig. 11 Shock standoff distance comparing multidomain spectral, single-domain spectral, and finite difference solutions as a function of distance along the surface of the cone for case V.

Case II

For the second problem, the heat transfer over a cylinder placed in an $M = 5.73$ freestream was computed, again using eight subdomains. This problem was also solved using a single domain in Ref. 9. Figure 6 shows the contours of the pressure, Mach number, and temperature along with the grid. As before, the solutions are smooth through the interfaces. The heat transfer along the surface of the cylinder as a function of the angle from the stagnation point is shown in Fig. 7. The results are compared with the experiments of Tiewfik and Geidt[14] and to the finite difference results of Gnoffo.[15] The heat transfer is sensitive to errors in the first derivatives of the temperature, making it a good test of a numerical method. Smoothness of the solution is implied by the continuity of the normal derivative of the temperature across the interfaces.

Case III

A more complex situation is shown in Fig. 8, which depicts the Mach 10.6 flow over a spherically blunted 150-deg half-angle cone. The solution contours in Fig. 8 show both the growth of the boundary layer along the cone surface and the shrinking of the entropy layer generated by the shock. The solution was computed on a grid of 14 subdomains. Figure 9 shows a comparison of the pressure coefficient along the surface of the cone to the inviscid calculation[5] and to the experimental results.[13] Marked by arrows on Fig. 9 are the positions of the subdomain interfaces.

Case IV

Case IV is similar to case III except that the temperature is kept fixed along the surface of the cone. Figure 10 shows the heat flux normalized to the value of the nose. The computed solution is compared with the experimental results.[13]

Case V

As a final example, we make more detailed comparisons of the results of an $M = 25$ flow over a 5-deg hyperbolic cone to those of the shock-fitted finite difference code of Ref. 12. The finite difference calculation used 50 points in each direction. Since the ideal gas law is used, the calculation is meant only for a comparison of the numerical results. This calculation used eight subdomains. Subdomains along the body used 13 points in the normal direction, whereas those along the shock used seven.

The calculation presented here required 140,000 time steps (starting with the inviscid solution) for the density to reduce the maximum residual in all flow variables 12 orders of magnitude. At 0.285 s per time step, this means that the calculation required approximately 11 h of CPU time on an IBM RS/6000 320H. For comparison purposes, this superscalar machine runs at approximately 4–5 Mflops. We will first compare the shock position and the wall values of the pressure coefficient, normalized heat transfer, and skin friction as a function of the distance s measured along the surface of the cone. We will also compare the profiles of the flow quantities in the direction

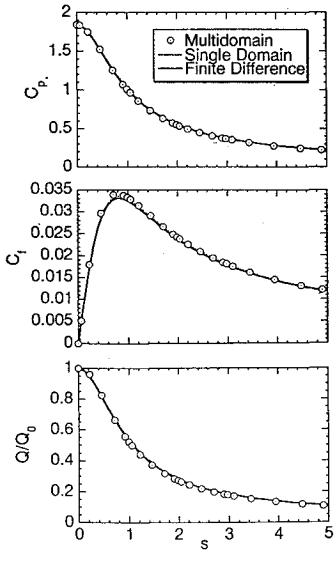

Fig. 12 Body surface quantities for case V.

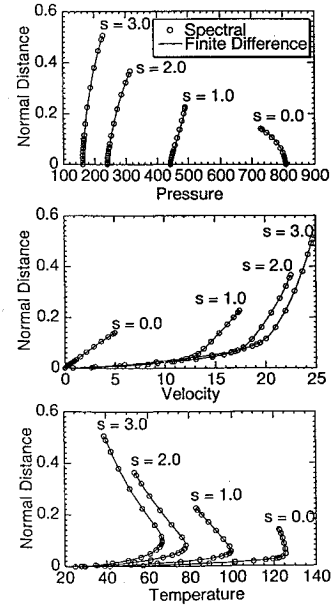

Fig. 13 Normal variation of flow quantities at four stations along the body for case V.

normal to the cone surface at four stations along the length of the cone. We begin by comparing the shock position, as shown in Fig. 11. Plotted is the normal distance of the shock from the body as a function of arclength along the body. Also compared with the multidomain solution is a single domain solution[9] computed on a 20×20 grid so that the number of points in the normal direction is the same.

Figure 12 compares the pressure coefficient, the heat flux Q, and the skin friction along the body surface as a function of the distance from the nose. Variations of the pressure, temperature, and velocity in the direction normal to the body surface are compared at four stations along the body in Fig. 13. The four stations correspond to the symmetry line and three interfaces that intersect the body. In all cases, we see excellent agreement between the spectral solution and the finite difference solution and smooth variations through the interfaces.

Conclusions

We have used a multidomain spectral collocation method to solve the compressible Navier–Stokes equations for two-dimensional and axisymmetric supersonic flows over blunt bodies. A main advantage of the method over a single domain method is the ability to distribute easily both subdomain boundary locations and the number of points in each subdomain. Thus, features such as boundary layers can be easily resolved.

At interfaces between subdomains, the advection terms are treated with the characteristic correction method used in Ref. 3 for the inviscid Euler equations. In this way, waves propagate through the interfaces in much the same way as they would for an inviscid flow. The diffusion terms are treated with a penalty method. The penalty weakly enforces the continuity of the viscous flux.

The method was applied to five problems. The computations show that the method is stable and that it converged in all cases to a smooth steady-state solution without the need for artificial viscosity or filtering. The results were compared with experimental data, with a finite difference solution, and with a single-domain spectral method.

Spectral methods are high-resolution methods and for smooth enough solutions give exponential order accuracy. Phase and dissipation errors are exponentially small. Along with the high accuracy, however, is the fact that the pointwise work is significantly higher than that required by low-order finite difference methods. This means that the computations are relatively expensive. Hanley[6] has presented evidence for one space dimension that if high enough accuracy is required, a spectral method can be as much as a factor of 7 more efficient than a second-order MacCormack scheme. Nevertheless, there is still a serious need for research on methods to accelerate the convergence rate of spectral methods. At this time, we consider the method described here to be appropriate for nose solutions. For longer bodies, the nose solution could be used as a starting solution for a marching code, since the approximation is defined by its Chebyshev interpolant even between grid points.

Acknowledgments

This research was supported in part NASA under Contract NAG1-862 and by the U.S. Department of Energy through Contract DE-FC05-85ER250000.

References

[1]Canuto, C., Hussaini, M. Y., Quarteroni, A., and Zang, T. A., *Spectral Methods in Fluid Mechanics*, Springer–Verlag, New York, 1987.

[2]Pruett, C. D., and Streett, C. L., "A Spectral Collocation Method for Compressible, Non-Similar Boundary Layers," *International Journal on Numerical Methods in Fluids*, Vol. 13, No. 6, 1991, pp. 713–737.

[3]Kopriva, D. A., "Multidomain Spectral Solution of the Euler Gas-Dynamics Equations," *Journal of Computational Physics*, Vol. 96, No. 2, 1991, pp. 428–450.

[4]Kopriva, D. A., "Spectral Solution of Inviscid Supersonic Flows over Wedges and Axisymmetric Cones," *Computers and Fluids*, Vol. 21, No. 2, 1992, pp. 247–266.

[5]Kopriva, D. A., "Spectral Solutions of High-Speed Flows over Blunt Cones," *AIAA Journal*, Vol. 31, No. 12, 1993, pp. 2227–2231.

[6]Hanley, P., "A Strategy for Efficient Simulation of Viscous Compressible Flows Using a Multi-Domain Pseudo-Spectral Method," *Journal of Computational Physics*, Vol 108, No. 1, 1993, pp. 153–158.

[7]Giannakourous, J., and Karniadakis, G. E., "A Spectral Element-FCT Method for the Compressible Euler Equations," *Journal of Computational Physics*, Vol. 115, No. 1, 1994, pp. 65–88.

[8]Kopriva, D. A., "Multidomain Spectral Solution of Compressible Viscous Flows," *Journal of Computational Physics*, Vol. 115, No. 1, 1994, pp. 184–198.

[9]Kopriva, D. A., "Spectral Solution of the Viscous Blunt Body Problem," *AIAA Journal*, Vol. 31, No. 7, 1993, pp. 1235–1242.

[10]Wang, J.-P., Nakamura, Y., and Yashuhara, M., "Global Coefficient Adjustment Method for Neuman Condition in Explicit Chebyshev Collocation Method and Its Application to Compressible Navier–Stokes Equations," *Journal of Computational Physics*, Vol. 107, No. 1, 1993, pp. 160–175.

[11]Moretti, G., and Salas, M. D., "The Blunt Body Problem for a Viscous Rarefied Gas Flow," AIAA Paper 69-139, Jan. 1969.

[12]Kumar, A., and Graves, R. A., "Numerical Solution of the Viscous Hypersonic Flow Past Blunted Cones at Angle of Attack," AIAA Paper 77-172, Jan. 1977.

[13]Cleary, J. W., "An Experimental and Theoretical Investigation of the Pressure Distribution and Flow Fields of Blunted Cones at Hypersonic Mach Numbers," NASA TN D-2969, 1965.

[14]Tewfik, O. K., and Giedt, W. H., "Heat Transfer, Recovery Factor, and Pressure Distributions Around a Circular Cylinder Normal to a Supersonic Rarefied-Air Stream," *Journal of the Aerospace Sciences*, Vol. 27, No. 10, 1960, pp. 721–729.

[15]Gnoffo, P. A., "Complete Supersonic Flowfields over Blunt Bodies in a Generalized Orthogonal Coordinate System," *AIAA Journal*, Vol. 18, No. 6, 1980, pp. 611, 612.